

# Spectroscopy of spin-orbit quantum bits in indium antimonide nanowires

S. Nadj-Perge,<sup>1</sup> V. S. Pribiag,<sup>1</sup> J. W. G. van den Berg,<sup>1</sup> K. Zuo,<sup>1</sup> S. R. Plissard,<sup>2</sup> E. P. A. M. Bakkers,<sup>1,2</sup> S. M. Frolov,<sup>1</sup> and L. P. Kouwenhoven<sup>1</sup>

<sup>1</sup>*Kavli Institute of Nanoscience, Delft University of Technology, 2600 GA Delft, The Netherlands*

<sup>2</sup>*Department of Applied Physics, Eindhoven University of Technology, 5600 MB Eindhoven, The Netherlands*

(Dated: April 18, 2022)

Double quantum dot in the few-electron regime is achieved using local gating in an InSb nanowire. The spectrum of two-electron eigenstates is investigated using electric dipole spin resonance. Singlet-triplet level repulsion caused by spin-orbit interaction is observed. The size and the anisotropy of singlet-triplet repulsion are used to determine the magnitude and the orientation of the spin-orbit effective field in an InSb nanowire double dot. The obtained results are confirmed using spin blockade leakage current anisotropy and transport spectroscopy of individual quantum dots.

PACS numbers: 73.63.Kv, 85.35.Be

The spin-orbit interaction (SOI) describes coupling between the motion of an electron and its spin. In one dimension, where electrons can move only to the left or to the right, the SOI couples this left or right motion to either spin-up or spin-down. An extreme situation occurs in what is called a helical liquid [1] where, in the presence of magnetic field, all spin-up electrons move to the left and all spin-down electrons to the right. As proposed recently [2, 3], a helical liquid in proximity to a superconductor can generate Majorana fermions [4]. The search for Majorana fermions in 1D conductors is focused on finding the best material in terms of a strong spin-orbit interaction and large Landé  $g$ -factors. The latter is required for a helical liquid to exist at magnetic fields that do not suppress superconductivity. High  $g$ -factors of the order 50, strong SOI and the ability to induce superconductivity put forward InSb nanowires [5, 6] as a natural platform for the realization of 1D topological states.

The SOI can be expressed as an effective magnetic field  $\vec{B}_{\text{SO}}$  that depends on the electron momentum. An electron moving through the wire undergoes spin precession around  $\vec{B}_{\text{SO}}$  with a  $\pi$  rotation over a distance  $l_{\text{SO}}$  called the spin-orbit length (see Fig. 1(a)). The length  $l_{\text{SO}}$  is a direct measure of the SOI strength: a stronger SOI results in a shorter  $l_{\text{SO}}$ . In this letter, we use spin spectra of single electrons in quantum dots [7] to extract  $l_{\text{SO}}$  and the direction of  $\vec{B}_{\text{SO}}$ . In quantum dots, the SOI hybridizes states with different spin [5, 8, 9]. For a single electron, the SOI-hybridized spin-up and spin-down states form a spin-orbit qubit [10, 11]. For two electrons SOI hybridization induces level repulsion between singlet and triplet states. The resulting level-repulsion gap between the well-defined qubit states can be used to measure the SOI: the gap size is determined by  $l_{\text{SO}}$  [5, 8, 9] and the gap anisotropy indicates the direction of  $\vec{B}_{\text{SO}}$  [12–14].

Double quantum dots in InSb nanowires are defined by local gating (Figs. 1(b),1(c)). A finite voltage is applied across the source and drain electrodes; and the current through the nanowire is measured. Five gates under-

neath the wire create the confinement potential and control the electron number on the two dots [9, 15]. We focus on the (1,1) charge configuration (Fig. 1(d)), in which both the left and the right dot contain exactly one electron, each of them representing a qubit [10, 11, 16–18].

The qubit eigenstates are described by the Kramers spin-orbit doublet  $\uparrow$  and  $\downarrow$ . These two states are superpositions of spin-up and spin-down, and of several of the lowest orbital states [20]. Similar to the case of pure spin states, a magnetic field  $B$  induces a Zeeman splitting  $E_Z = g\mu_B B$  between the Kramers doublets, where  $g$  is the effective Landé  $g$ -factor for a given direction of  $\vec{B}$ , and  $\mu_B$  is the Bohr magneton. The two qubits in the (1,1) configuration can either form a Kramers singlet state S(1,1) or one of the three triplets  $T_+(1,1)$ ,  $T_0(1,1)$  and  $T_-(1,1)$ . The states of the qubits are prepared using Pauli spin blockade [10, 11, 17, 18, 21] (Fig. 2(a)), which relies on the tunneling process from (1,1) to the (0,2) spin singlet S(0,2) (note that T(0,2) state is at 5 meV above S(0,2) and therefore inaccessible for  $B = 0$ ). When the two electrons form a triplet state, tunneling of the left electron to the right dot is prohibited by selection rules. This absence of tunneling initializes the qubits in the so-called blocked (1,1) state and thereby suppresses the current of electrons passing through the double dot. Leakage current can occur due to hybridization of T(1,1) states with S(0,2) induced by SOI and by spin mixing between T(1,1) and S(1,1) due to hyperfine interaction [8, 15, 22, 23].

Transitions between qubit states are induced by a.c. electric fields via electric dipole spin resonance (EDSR) [10, 11, 16, 25–27]. Voltages at microwave frequencies are applied to the left plunger (LP) gate (Fig. 2(a)). The oscillating electric field wiggles the electronic orbits. This periodic motion results, via SOI, in a rotation of the spin [10, 11]. When the microwave frequency is on resonance with the double dot level transitions, EDSR can assist in overcoming spin blockade thereby increasing the current through the double dot. We map out this current increase as a function of microwave frequency  $f$  and  $\vec{B}$  (Fig. 2(b)).

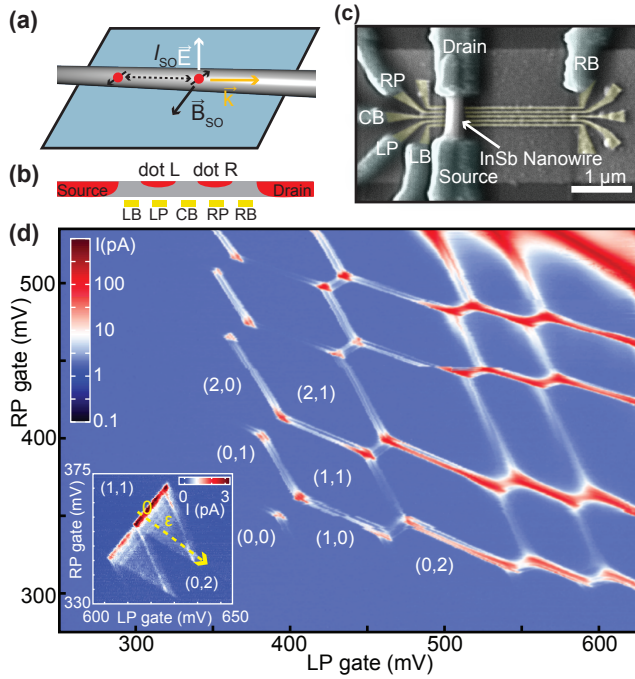


FIG. 1: (color online) (a), An electron moving with momentum  $\vec{k}$  through the wire experiences a spin-orbit field  $\vec{B}_{SO}$  which rotates the spin by  $\pi$  after a distance  $l_{SO}$ . Vector  $\vec{E}$  indicates likely direction of the electric field. In the case of spin-orbit coupling due to structural inversion asymmetry,  $\vec{B}_{SO} \propto \vec{E} \times \vec{k}$  [19]. (b), Schematic of a double quantum dot in an InSb nanowire. Red color indicates regions of the nanowire which are not depleted by gates. Gates LB, CB, and RB define the left, central and right barriers. Gates LP and RP are the left and right plungers used to control the electron number on each dot. (c), Scanning electron microscopy of a nanowire device similar to the one used in the measurements. (d), Charge stability diagram of the double dot for source-drain voltage  $V_{sd} = 1$  mV. Typical charging energy is 10 meV. Numbers in brackets correspond to the charge occupation on the left and the right dots. The inset shows the charge stability diagram near the (1,1)  $\rightarrow$  (0,2) charge transition for  $V_{sd} = 5$  mV. The detuning axis  $\varepsilon$  is indicated by the dashed arrow.

For weak interdot tunnel coupling the spectrum is determined by the energies of individual qubits. At  $B=0$  all four states are degenerate and non-blocked due to fast decay to singlet state induced by hyperfine interaction [22]. At finite  $B$ , parallel configurations  $(\uparrow, \uparrow) = T_+(1,1)$  and  $(\downarrow, \downarrow) = T_-(1,1)$  split in energy and become blocked, while the other two configurations  $(\downarrow, \uparrow)$  and  $(\uparrow, \downarrow)$  remain non-blocked. EDSR induces transitions between ‘parallel’ and ‘anti parallel’ configurations, resulting in an on-resonance current as observed in Fig. 2(b). The slopes of the two “V” shaped resonances determine the  $g$ -factors of the right and left dots,  $|g_R| = 29.7 \pm 0.2$  and  $|g_L| = 32.2 \pm 0.2$  for this plot. Moreover, the  $g$ -factors of both dots are highly anisotropic as revealed by the EDSR spectroscopy for different field orientations (Fig.

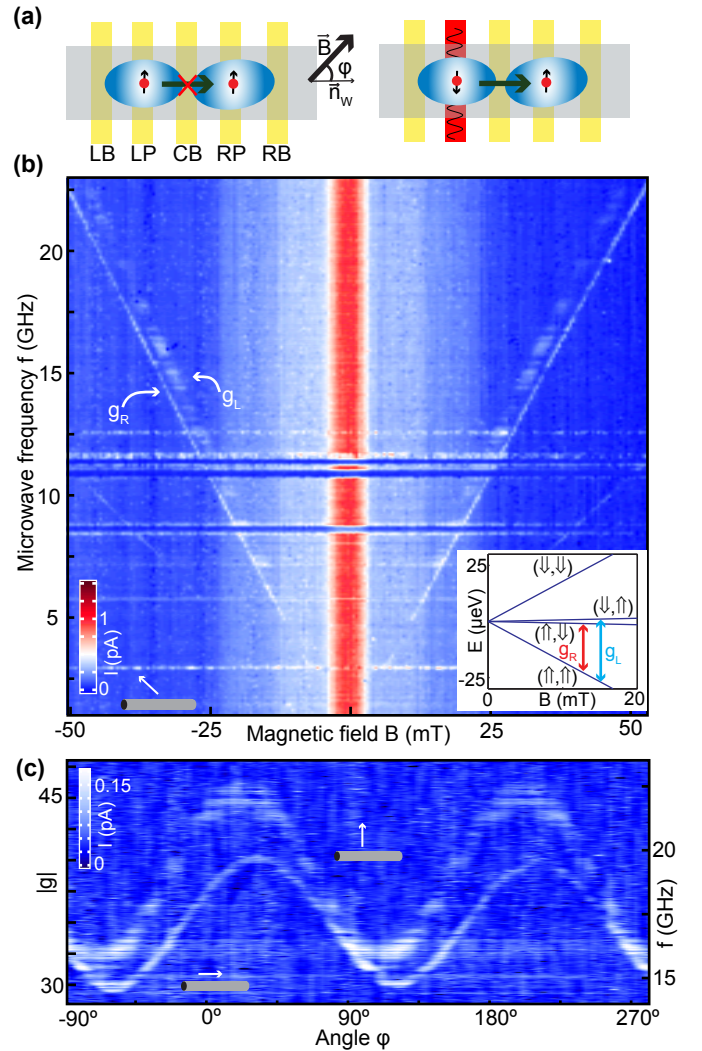


FIG. 2: (color online) (a), Left: blocked parallel configuration.  $\varphi$  is the angle between nanowire axis  $\vec{n}_W$  and  $\vec{B}$ . Right: microwaves applied to LP gate (red) induce EDSR. Tunneling to the right dot is allowed when the left qubit is rotated to antiparallel configuration. (b) V-shaped EDSR resonances with slopes providing  $g_L$  and  $g_R$  for  $\varphi = 130^\circ$  and  $V_{sd} = 8$  mV. Larger  $g$ -factor was assigned to the larger dot, i.e. to the dot with smaller orbital energy (orbital energy is 5 meV for the left dot and 7.5 meV for the right dot). V-shaped lines with half the slope are two-photon transitions. Enhanced current around  $B=0$  is due to spin mixing in the absence of microwaves (see [24] section S2). Resonances at constant  $f$  are due to photon-assisted tunneling enhanced by cavity modes. (At each frequency the maximum current is normalized to 1pA and a constant offset is subtracted for clarity.) Inset shows energy spectrum of weakly coupled double dots with arrows illustrating the observed transitions. (c), Current versus  $f$  and  $\varphi$  for  $B = 35$  mT. Vertical axis on the left is rescaled to  $g = hf / \mu_B B$ . (At each field a constant current offset is subtracted for clarity.) White arrows over grey cylinders indicate B-field orientation with respect to nanowire in panels (b) and (c).

2(c)). The observed anisotropy is likely determined by the details of confinement [28, 29] since the  $g$ -factor in bulk zincblende InSb is expected to be isotropic.

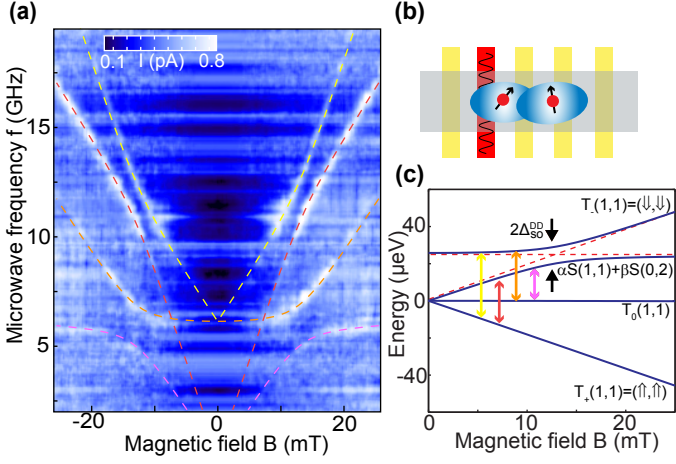


FIG. 3: (color online) (a), Current, in color, versus  $f$  and  $B$  for detuning  $\varepsilon \approx 0.5$  meV ( $V_{sd} = -5$  mV). Dashed lines are fits to a model described in the [24] section S4. Line colors match transitions indicated in panel (c). (At each frequency a current offset is subtracted for clarity.) (b), Diagram illustrating a strongly coupled double quantum dot realized by applying a more positive voltage to the central gate. (c), Energy diagram deduced from (a) and used to extract the S-T spin-orbit gap  $\Delta_{SO}^{DD}$ . Arrows indicate transitions observed in (a). In the absence of coupling, the triplet and the singlet state would simply cross as indicated by dashed lines.

When we increase the interdot tunneling (Fig. 3(b)), the (1,1) states hybridize with  $S(0,2)$  resulting in level repulsion between spectral lines. In the absence of SOI, only states with the same spin can hybridize *e.g.*  $S(1,1)$  with  $S(0,2)$ . SOI, however, also enables hybridization between the singlets and the triplets [7, 9, 23, 30] (Fig. 3; see also Fig. 4(e)). All observed transitions in Fig. 3(a) can be identified using a simple model which takes into account the hybridization between the (1,1) triplets and  $S(0,2)$  (see [24] section S4). The four avoided crossings observed in Fig. 3(a) correspond to the same double dot spin-orbit gap  $\Delta_{SO}^{DD}$  between  $T_{\pm}(1,1)$  and the singlet, as illustrated in Fig. 3(c). The quantitative comparison with the model allows us to estimate the spin-orbit length  $l_{SO} = 230 \pm 40$  nm (see [24] section S5).

The observed singlet-triplet gap is highly anisotropic (Fig. 4). The gap  $\Delta_{SO}^{DD}$  is largest when  $\vec{B}$  is parallel to the nanowire axis  $\vec{n}_W$ :  $\Delta_{SO}^{DD}$  shrinks as the direction of  $\vec{B}$  is rotated in the sample plane (Fig. 4(b) and 4(c)). Finally for  $\vec{B} \perp \vec{n}_W$  the gap disappears (Fig. 4(d)). For this orientation the resonance line corresponding to the  $T_{+}(1,1)$  to singlet transition becomes straight indicating the absence of level repulsion between  $T_{-}(1,1)$  and singlet. In addition, the visibility of the  $T_{+}(1,1) \rightarrow T_{\pm}(1,1)$  transition vanishes, suggesting that both  $T_{+}(1,1)$  and  $T_{\pm}(1,1)$  states are completely blocked for this field orientation.

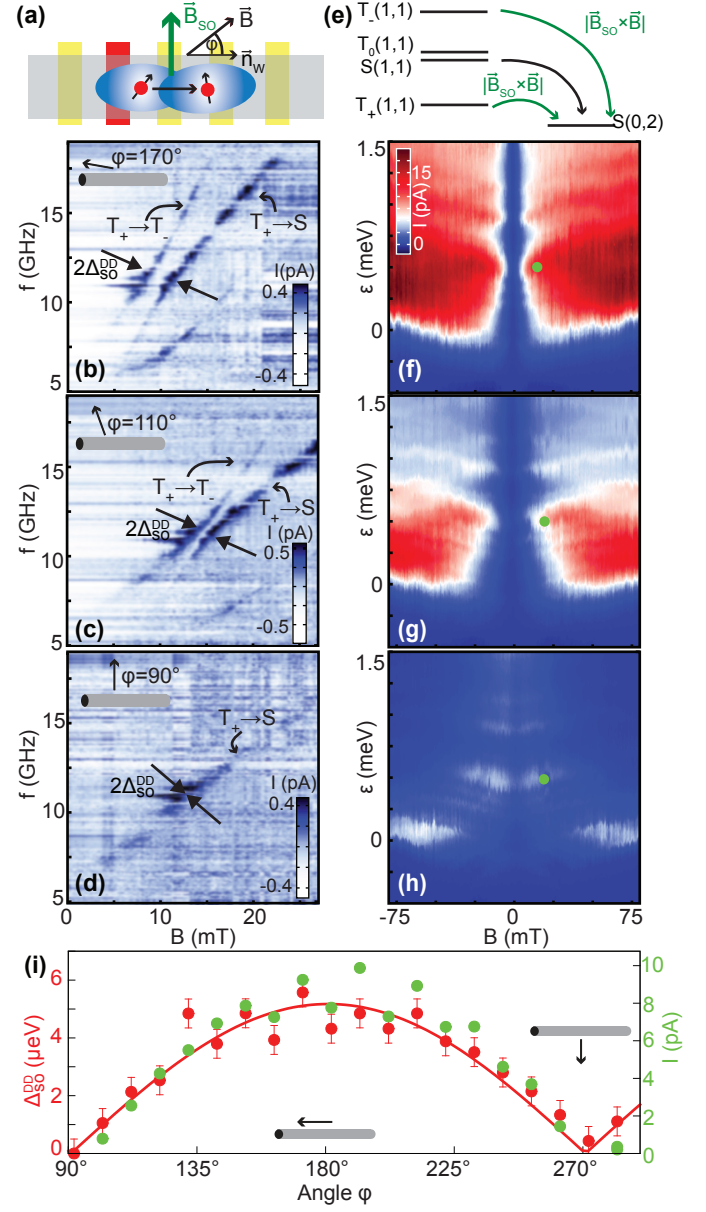


FIG. 4: (color online) a, As the left electron tunnels to the right it experiences a field  $\vec{B}_{SO}$ . (b-d) The avoided crossing in the EDSR spectrum as in Fig. 3(a) for three directions of  $\vec{B}$ :  $\varphi = 170^\circ$ ;  $\varphi = 110^\circ$ ; and  $\varphi = 90^\circ$  ( $V_{sd} = -5$  mV). (At each magnetic field an offset is subtracted for clarity.) (e), Transitions between (1,1) states and  $S(0,2)$  at finite  $B$ . The two singlet states are hybridized due to tunnel coupling.  $T_{+}(1,1)$  and  $T_{-}(1,1)$  are coupled to  $S(0,2)$  due to  $\vec{B}_{SO}$ . This SOI induced coupling scales as  $|\vec{B}_{SO} \times \vec{B}|$  for small  $\vec{B}$  [23]. (f-h),  $I$  versus  $\varepsilon$  and  $B$  for the same orientations of  $\vec{B}$  as in (b-d) with microwaves off. (i), Extracted values of  $\Delta_{SO}^{DD}$  (see [24] section S6) and  $I$  at  $B = 20$  mT and  $\varepsilon = 0.5$  meV (green dot in panels (f-h)) as a function of  $\varphi$ . Solid line is a fit to  $\Delta_{SO}^{DD} = \Delta_{SO} |\cos(\varphi - \varphi_0)|$  with  $\Delta_{SO} = 5.2 \pm 0.3$   $\mu\text{eV}$  and  $\varphi_0 = 1^\circ \pm 5^\circ$ . The error bars are determined by the width of EDSR resonance.

The observed anisotropy of  $\Delta_{SO}^{DD}$  confirms the spin-



orbit origin of the singlet-triplet level repulsion (see also [24] section S3). The gap  $\Delta_{\text{SO}}^{\text{DD}}$  is expected to be proportional to  $|\vec{B}_{\text{SO}} \times (\vec{B}/B)|$  [23, 31, 32]. When the two fields are aligned, singlet and triplet states cannot mix and therefore the spin-orbit gap closes (Fig. 4(d)). From the observed anisotropy we conclude that  $\vec{B}_{\text{SO}}$  points perpendicular to the nanowire and is parallel to the substrate plane (Figs. 4(i) and 4(a)).

The knowledge of  $\vec{B}_{\text{SO}}$  orientation provides a substantial increase in the fidelity of the initialization and readout of spin-orbit qubits [10]. The fidelity is presently limited due to unwanted transitions from  $T_+(1,1)$  and  $T_-(1,1)$  to  $S(0,2)$  induced by SOI. When  $\vec{B}$  and  $\vec{B}_{\text{SO}}$  are misaligned,  $T_+(1,1)$  and  $T_-(1,1)$  are coupled to  $S(0,2)$  (Fig. 4(e)) [23]. The unwanted transitions are manifest in the d.c. current through the double dot at finite magnetic fields (Figs. 4(f), 4(g), 4(h)) [15, 30]. For an ideal readout and initialization no current flows after either  $T_+(1,1)$  or  $T_-(1,1)$  state is occupied. When  $\vec{B}$  is aligned with  $\vec{B}_{\text{SO}}$ ,  $T_+(1,1)$  and  $T_-(1,1)$  become decoupled from  $S(0,2)$  and d.c. current is expected to vanish. This dramatic suppression of d.c. current is observed for  $\vec{B} \perp \vec{n}_W$  (Fig. 4(h)). Importantly, both  $\Delta_{\text{SO}}^{\text{DD}}$  and  $I$  show almost identical angle dependence further confirming that the singlet-triplet hybridization due to SOI is absent when  $\vec{B} \parallel \vec{B}_{\text{SO}}$  (Fig. 4(i)).

Given the direction of  $\vec{B}_{\text{SO}}$  we can analyze the origin of the spin-orbit interaction in InSb nanowires. The field  $\vec{B}_{\text{SO}}$  depends on the electron momentum  $\vec{k}$ . In a simple physical picture, during the interdot tunneling, the momentum  $\vec{k}$  is along the nanowire, which is grown in the [111] crystallographic direction. In zincblende InSb the spin-orbit interaction has two contributions, the bulk-inversion asymmetry term (BIA) and the structure-inversion asymmetry term (SIA). However, for  $\vec{k} \parallel [111]$  the BIA term is expected to vanish [19], and therefore the SIA contribution should dominate. The field  $\vec{B}_{\text{SO}}$  due to SIA is orthogonal to both the momentum and the external electric field (Fig. 1(c)). The electric field is likely perpendicular to the substrate since the symmetry of confinement in the nanowire is broken by the substrate dielectric and voltages on the gates. Therefore the direction  $\vec{B}_{\text{SO}} \perp \vec{n}_W$  and in the substrate plane is consistent with the SIA spin-orbit interaction.

We compare the results obtained from EDSR spectroscopy with the spectrum of (0,2) states (Fig. 5(a)) [5, 9, 30]. The SOI hybridization of  $S(0,2)$  and  $T_+(0,2)$  states leads to a single dot spin-orbit gap  $\Delta_{\text{SO}}^{\text{SD}}$ . Since the energies of the (0,2) states are too large to be accessed with microwaves ( $\Delta_{\text{ST}} \approx 5$  meV at  $B=0$ ), we use the lowest energy  $T_+(1,1)$  level as a probe of the (0,2) spectrum. By changing detuning we move  $T_+(1,1)$  with respect to the (0, 2) levels. When  $T_+(1,1)$  is aligned with either  $S(0,2)$  or  $T_+(0,2)$ , an increase in d.c. current is observed (Fig. 5(b)) [8]. The level repulsion between  $T_+(0,2)$  and

$S(0,2)$  is observed at  $B \approx 2T$  (Fig. 5(c)). The single dot gap is also strongly anisotropic reaching the smallest value for  $\vec{B} \perp \vec{n}_W$  (Figs. 5(d), 5(e) and 5(f)). The spin-orbit length  $l_{\text{SO}} = 310 \pm 50$  nm estimated from  $\Delta_{\text{SO}}^{\text{SD}}$  is in agreement with the value obtained using EDSR.

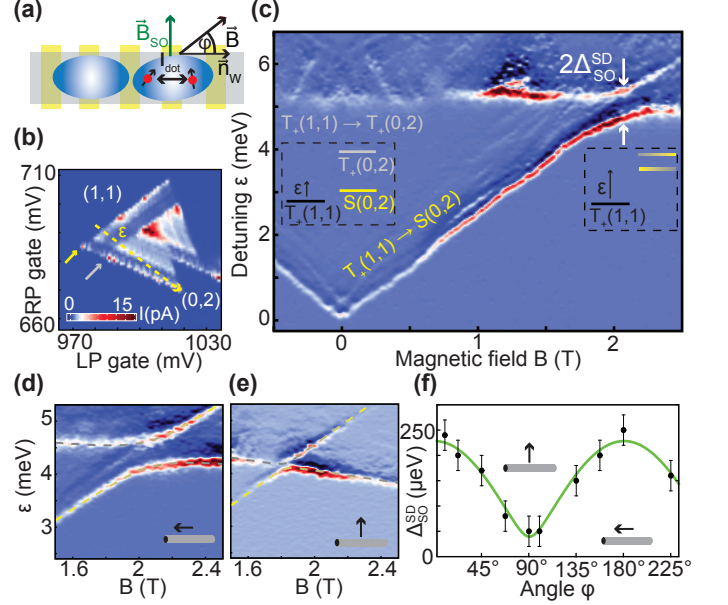


FIG. 5: (color online) (a), Two electrons in the right quantum dot. The separation of the two electrons in the triplet state is of the order of the dot size. (b), Charge stability diagram close to  $(1,1) \rightarrow (0,2)$  transition at  $B=1.4$  T, for  $V_{sd}=7$  mV and  $\vec{B} \parallel \vec{n}_W$ . Transitions  $T_+(1,1) \rightarrow S(0,2)$  and  $T_+(1,1) \rightarrow T_+(0,2)$  are indicated by yellow and gray arrows. (c), Resonances corresponding to  $T_+(1,1) \rightarrow S(0,2)$  and  $T_+(1,1) \rightarrow T_+(0,2)$  as a function of  $B$  for  $\varphi=180^\circ$ . Colors from dark blue (low) to red (high) in panes (c), (d) and (e) indicate values of  $dI/d\varepsilon$  in arbitrary units. (d) and (e), Avoided crossing for  $\varphi=180^\circ$  and  $\varphi=90^\circ$ . The dashed lines are fits to the model from Ref. [9]. (f), The gap  $\Delta_{\text{SO}}^{\text{SD}}$  as a function of  $\varphi$ . Solid line is a fit to  $\Delta_{\text{SO}}^{\text{SD}} = \Delta'_{\text{SO}} \sqrt{\cos^2(\varphi - \varphi_0) \cos^2 \theta + \sin^2 \theta}$  with  $\Delta'_{\text{SO}} = 230 \pm 10$   $\mu\text{eV}$ ,  $\varphi_0 = 2^\circ \pm 5^\circ$  and  $\theta = 10^\circ \pm 3^\circ$ . The error bars are determined by average linewidth corresponding to  $T_+(1,1) \rightarrow S(0,2)$  and  $T_+(1,1) \rightarrow T_+(0,2)$  transitions. Note that the anisotropy of  $\Delta_{\text{SO}}^{\text{SD}}$  depends on the relative positions of the two electrons in the right dot which may be different from nanowire axis. Out-of-plane  $\vec{B}_{\text{SO}}$  angle  $\theta$  therefore may be non-zero due to confinement details of the right quantum dot. Measurements at the  $(1,1) \rightarrow (2,0)$  transition yielded the same in-plane anisotropy for the left dot (data not shown).

We can now assess the potential of InSb nanowires for the experimental observation of Majorana bound states in hybrid nanowire-superconductor devices [2, 3]. Majorana states are expected to appear at the boundaries of the topological superconducting phase. The topological phase is predicted to occur if: (i)  $E_Z > \Delta$  and (ii)  $E_{\text{top}}, \Delta > T$ . Here  $\Delta$  is the superconducting gap,  $E_{\text{top}}$  is the gap of the topological phase and  $T$  is the temperature. Due to the large  $g$ -factors in InSb nanowires the first re-

quirement can be satisfied at low magnetic fields even for large gap superconductors such as niobium ( $\Delta \sim 5\text{K}$ ). The size of the topological gap  $E_{\text{top}} \approx 2\sqrt{E_{\text{SO}}\Delta}$  is determined by the bulk SOI splitting  $E_{\text{SO}} = \hbar^2/(2m_e^*l_{\text{SO}}^2)$  [1]. Here  $\hbar$  is the Planck constant and  $m_e^* \approx 0.015m_e$  is the effective electron mass ( $m_e$  is the electron mass). We estimate  $E_{\text{SO}} \approx 0.5\text{ K}$  and  $E_{\text{top}} \approx 3\text{ K}$  for the case of ballistic one-dimensional transport. The orientation  $\vec{B} \parallel \vec{n}_W$  is optimal for observing Majorana states since the maximum mixing of the SOI-split bands occurs for  $\vec{B} \perp \vec{B}_{\text{SO}}$  and the superconductivity is suppressed least when  $\vec{B}$  is in the substrate plane.

We would like to thank J. Danon, Y. Nazarov, M. Rudner, D. Loss, F. Hassler and J. van Tilburg for discussions and help. We acknowledge help with the measurement software from R. Heeres and P. de Groot. This work has been supported by ERC, NWO/FOM Netherlands Organization for Scientific Research and through the DARPA program QUEST.

- 
- [1] Středa, P. and Šeba, P., *Phys. Rev. Lett.* **90**, 256601 (2003).
- [2] Lutchyn, R. M., Sau, J. D., and Das Sarma, S., *Phys. Rev. Lett.* **105**, 077001 (2010).
- [3] Oreg, Y., Refael, G., and von Oppen, F., *Phys. Rev. Lett.* **105**, 177002 (2010).
- [4] Kitaev, A. Y., *Physics-Uspekhi* **44**(10S), 131 (2001).
- [5] Nilsson, H. A., Caroff, P., Thelander, C., Larsson, M., Wagner, J. B., Wernersson, L.-E., Samuelson, L., and Xu, H. Q., *Nano Letters* **9**, 3151 (2009).
- [6] Nilsson, H. A., Samuelsson, P., Caroff, P., and Xu, H. Q., *Nano Letters* (2011).
- [7] Schreiber, L. R., Braakman, F., Meunier, T., Calado, V., Danon, J., Taylor, J. M., Wegscheider, W., and Vandersypen, L. M. K., *Nature Communications* **2**, 556 (2011).
- [8] Pfund, A., Shorubalko, I., Ensslin, K., and Leturcq, R., *Phys. Rev. B* **76**, 161308 (2007).
- [9] Fasth, C., Fuhrer, A., Samuelson, L., Golovach, V. N., and Loss, D., *Phys. Rev. Lett.* **98**, 266801 (2007).
- [10] Nadj-Perge, S., Frolov, S. M., Bakkers, E. P. A. M., and Kouwenhoven, L. P., *Nature* **468**, 1084 (2010).
- [11] Nowack, K. C., Koppens, F. H. L., Nazarov, Y. V., and Vandersypen, L. M. K., *Science* **318**, 1430 (2007).
- [12] Takahashi, S., Deacon, R. S., Yoshida, K., Oiwa, A., Shibata, K., Hirakawa, K., Tokura, Y., and Tarucha, S., *Phys. Rev. Lett.* **104**, 246801 (2010).
- [13] Kanai, Y., Deacon, R. S., Takahashi, S., Oiwa, A., Yoshida, K., Shibata, K., Hirakawa, K., Tokura, Y., and Tarucha, S., *Nat Nano* **6**, 511 (2011).
- [14] Golovach, V. N., Khaetskii, A., and Loss, D., *Phys. Rev. B* **77**, 045328 (2008).
- [15] Nadj-Perge, S., Frolov, S. M., van Tilburg, J. W. W., Danon, J., Nazarov, Y. V., Algra, R., Bakkers, E. P. A. M., and Kouwenhoven, L. P., *Phys. Rev. B* **81**, 201305(R) (2010).
- [16] Pioro-Ladriere, M., Obata, T., Tokura, Y., Shin, Y. S., Kubo, T., Yoshida, K., Taniyama, T., and Tarucha, S., *Nature Physics* **4**, 776 (2008).
- [17] Petta, J. R., Johnson, A. C., Taylor, J. M., Laird, E. A., Yacoby, A., Lukin, M. D., Marcus, C. M., Hanson, M. P., and Gossard, A. C., *Science* **309**, 2180 (2005).
- [18] Koppens, F. H. L., Buizert, C., Tielrooij, K. J., Vink, I. T., Nowack, K. C., Meunier, T., Kouwenhoven, L. P., and Vandersypen, L. M. K., *Nature* **442**, 766 (2006).
- [19] Winkler, R., *Spin-Orbit Coupling Effects in Two-Dimensional Electron and Hole Systems*. Springer, Berlin, (2003).
- [20] Flindt, C., Sorensen, A. S., and Flensberg, K., *Phys. Rev. Lett.* **97**, 240501 (2006).
- [21] Ono, K., Austing, D. G., Tokura, Y., and Tarucha, S., *Science* **297**, 1313 (2002).
- [22] Koppens, F. H. L., Folk, J. A., Elzerman, J. M., Hanson, R., van Beveren, L. H. W., Vink, I. T., Tranitz, H. P., Wegscheider, W., Kouwenhoven, L. P., and Vandersypen, L. M. K., *Science* **309**, 1346 (2005).
- [23] Danon, J. and Nazarov, Y. V., *Phys. Rev. B* **80**, 041301 (2009).
- [24] Supplementary Material accompanies this paper.
- [25] Bell, R. L., *Phys. Rev. Lett.* **9**, 52 (1962).
- [26] Golovach, V. N., Borhani, M., and Loss, D., *Phys. Rev. B* **74**, 165319 (2006).
- [27] Laird, E. A., Barthel, C., Rashba, E. I., Marcus, C. M., Hanson, M. P., and Gossard, A. C., *Phys. Rev. Lett.* **99**, 246601 (2007).
- [28] Pryor, C. E. and Flatté, M. E., *Phys. Rev. Lett.* **96**, 026804 (2006).
- [29] Schroer, M. D., Petersson, K. D., Jung, M., and Petta, J. R., *Phys. Rev. Lett.* **107**, 176811 (2011).
- [30] Pfund, A., Shorubalko, I., Ensslin, K., and Leturcq, R., *Phys. Rev. Lett.* **99**, 036801 (2007).
- [31] Nowak, M. P., Szafran, B., Peeters, F. M., Partoens, B., and Pasek, W. J., *Physical Review B* **83**, 245324 (2011).
- [32] Stepanenko, D., Rudner, M., Halperin, B. I., and Loss, D., *unpublished*, [arXiv:1112.1644](https://arxiv.org/abs/1112.1644) (2011).